



# lncRNA H19 prevents endothelial–mesenchymal transition in diabetic retinopathy

Anu A. Thomas<sup>1</sup> · Saumik Biswas<sup>1</sup> · Biao Feng<sup>1</sup> · Shali Chen<sup>1</sup> · John Gonder<sup>2</sup> · Subrata Chakrabarti<sup>1</sup>

Received: 11 July 2018 / Accepted: 15 November 2018 / Published online: 5 January 2019  
© Springer-Verlag GmbH Germany, part of Springer Nature 2018

## Abstract

**Aims/hypothesis** The pathophysiology of diabetic retinopathy is linked to hyperglycaemia and its effect on retinal microvascular tissues. The resulting endothelial injury changes the endothelial cell phenotype to acquire mesenchymal properties (i.e. endothelial–mesenchymal transition [EndMT]). Such changes can be regulated by epigenetic mechanisms, including long non-coding RNAs (lncRNAs). lncRNA H19 may influence EndMT through TGF- $\beta$ . We investigated the role of H19 in regulating EndMT during diabetic retinopathy.

**Methods** H19 was overexpressed or silenced in human retinal endothelial cells exposed to various glucose levels. The cells were examined for H19, endothelial and mesenchymal markers. We then expanded the study to retinal tissues in a mouse model of diabetic retinopathy and also examined vitreous humour samples from individuals with proliferative diabetic retinopathy.

**Results** Expression of H19 was downregulated in high glucose conditions (25 mmol/l). H19 overexpression prevented glucose-induced EndMT. Such changes appear to involve TGF- $\beta$  through a Smad-independent mechanism. Diabetes caused downregulation of retinal H19. Using *H19* knockout mice, we demonstrated similar EndMT in the retina. Examination of vitreous humour from individuals with proliferative diabetic retinopathy also reinforced the downregulation of H19 in diabetes.

**Conclusions/interpretation** We therefore concluded that H19 regulates EndMT in diabetic retinopathy through specific mechanisms.

**Data availability** The results from our previous microarray can be found online using the GEO accession number GSE122189.

**Keywords** Diabetic retinopathy · Endothelial–mesenchymal transition · H19 · TGF- $\beta$

## Abbreviations

ECM	Extracellular matrix	HG	High D-glucose (25 mmol/l) (experimental treatment)
EMT	Epithelial–mesenchymal transition	HRECs	Human retinal microvascular endothelial cells
EndMT	Endothelial–mesenchymal transition	KO	Knockout
ERK	Extracellular signal-regulated kinase	lncRNA	Long non-coding RNA
FISH	Fluorescence in situ hybridisation	MAPK	Mitogen-activated protein kinase
FSP1	Fibroblast-specific protein 1	miR	microRNA
GEO	Gene Expression Omnibus	NG	Normal D-glucose (5 mmol/l) (experimental treatment)
		NIH	National Institutes of Health
		PDR	Proliferative diabetic retinopathy
		PI3K	Phosphatidylinositol-3-kinase
		SM22	Smooth muscle 22
		$\alpha$ -SMA	$\alpha$ -Smooth muscle actin
		STZ	Streptozotocin
		TGF $\beta$ RII	TGF- $\beta$ receptor II
		VE-cad	Vascular endothelial cadherin
		VEGF	Vascular endothelial growth factor

**Electronic supplementary material** The online version of this article (<https://doi.org/10.1007/s00125-018-4797-6>) contains peer-reviewed but unedited supplementary material, which is available to authorised users.

✉ Subrata Chakrabarti  
subrata.chakrabarti@lhsc.on.ca

<sup>1</sup> Department of Pathology and Laboratory Medicine, Western University, Dental Science Building 4033, 1151 Richmond Street, London, ON N6A 5C1, Canada

<sup>2</sup> Department of Ophthalmology, Western University, London, ON, Canada

## Research in context

### What is already known about this subject?

- Glucose induces cellular phenotypic changes known as endothelial–mesenchymal transition (EndMT)
- Both EndMT and epithelial–mesenchymal transition are activated by TGF- $\beta$  signalling pathways
- Long non-coding RNA (lncRNA) H19 can regulate epithelial–mesenchymal transition mediated by other epigenetic regulators such as microRNA (miR)-200 and histone modifiers

### What is the key question?

- Does lncRNA H19 regulate glucose-induced EndMT through specific TGF- $\beta$  and miRNA-200b signalling pathways?

### What are the new findings?

- lncRNA H19 prevents glucose-induced EndMT and may work independently of miRNA-200b
- H19 facilitates this regulation by suppressing TGF- $\beta$  and its MAPK–ERK1/2 signalling pathway

### How might this impact on clinical practice in the foreseeable future?

- In this study, we have shown that lncRNA H19 is downregulated on glucose exposure and regulates key cellular phenotypic alterations (EndMT) during diabetic retinopathy. This understanding can contribute to future development of RNA-based or other epigenetic mechanism-based therapies for complications of chronic diabetes

## Introduction

Diabetes mellitus leads to several life-limiting complications, and its worldwide prevalence is estimated to rise from 382 million in 2013 to 592 million by 2035 [1, 2]. Diabetic retinopathy, a prominent microvascular complication, causes vision-threatening retinal changes in one-third of the diabetic population [3]. Progression of diabetic retinopathy is associated with duration of diabetes, hypertension and hyperglycaemia [4], and hyperglycaemia has been shown to impair endothelial function in animal and human studies [5, 6].

Endothelial cells lining the circulatory system facilitate effective blood pumping, regulate coagulation, fibrinolysis, platelet aggregation and vascular tone, and play critical roles in maintaining homeostasis [7]. In hyperglycaemia, endothelial cells undergo a range of intracellular events that promote endothelial dysfunction and loss of physiological properties [7]. In diabetes, dysfunctional endothelial cells promote excess accumulation of extracellular matrix (ECM) proteins in damaged tissues, leading to organ dysfunction [8, 9]. Accumulation of ECM is accompanied by fibroblast proliferation and its differentiation into myofibroblasts, the key cellular mediators of fibrosis [10]. Damaged endothelial cells express markers characteristic of myofibroblast differentiation such as  $\alpha$ -smooth muscle actin ( $\alpha$ -SMA), smooth muscle 22 (SM-22), vimentin and fibroblast-specific protein 1 (FSP1), thereby adopting a mesenchymal phenotype [11]. Concurrently, endothelial cell markers such as vascular endothelial (VE)-cadherin and CD31 are downregulated [11]. This phenomenon, known as endothelial–mesenchymal transition (EndMT), which results

in a differentiated phenotype, imparts invasive and migratory abilities to affect pathological processes [11].

Switching of cellular phenotypes is an important biological event, and phenotypic alterations from epithelial to mesenchymal cell type, termed epithelial–mesenchymal transition (EMT), is a key paradigm during embryonic development [11, 12]. It is classified into three categories: type 1 EMT occurs during the embryonic and developmental stages, and types 2 and 3 EMT are active after birth and are involved with fibrosis in chronic inflammation and malignancies, respectively [11]. EndMT can be considered as a subcategory of EMT and associated with its three categories [11]. EndMT involves phenotypic changes, evidenced by a decrease in endothelial markers and an increase in mesenchymal markers. EMT, on the other hand, is characterised by a decrease in epithelial cell markers (e.g. E-cadherin and integrins) and an increase in mesenchymal markers [11, 13]. EndMT, similar to EMT, may be regulated by the TGF- $\beta$  superfamily of proteins, including TGF- $\beta$ 1 and TGF- $\beta$ 2, through Smad-dependent and Smad-independent signalling pathways such as MAPK/ERK kinase (MEK)–extracellular signal-regulated kinase (ERK), phosphatidylinositol-3-kinase (PI3K) and p38 mitogen-activated protein kinase (MAPK) [11, 14, 15].

Long non-coding RNAs (lncRNAs) are RNA transcripts (>200 nucleotides) that lack protein-coding potential [16]. lncRNAs play important roles in physiological processes, for example as modulators of alternative splicing, factors involved in chromatin remodelling and *cis/trans*-acting regulators of gene expression and RNA metabolism [17, 18]. Recent evidence shows that dysregulation of target genes leads to

abnormal lncRNA expression in multiple cancer types and plays a critical role in mediating TGF- $\beta$ -induced EMT during tumour metastasis [19, 20]. One key lncRNA in tumorigenesis is the oncofetal lncRNA H19. The *H19* gene is paternally imprinted and produces a 2.3 kb spliced, capped and polyadenylated lncRNA, which is predominantly cytoplasmic and co-regulated by insulin-like growth factor 2, a maternally imprinted gene located at the same locus [21]. Specific roles of H19 in tumorigenesis are disputable as it harbours pro-tumorigenic [22] and tumour-suppressive [21, 23] properties. In diabetes, exposure to high glucose levels reduced H19 expression in neonatal cardiomyocytes, and in the myocardium of streptozotocin (STZ)-induced diabetes in rats used as a model of diabetes [24]. H19 has also been shown to alter the microRNA (miR)-200 pathway by increasing upstream histone acetylation, thus reversing EMT [23]. We have previously documented that, without affecting other members of the miR-200 family (miR-200a and miR-429), miR-200b is specifically downregulated in the retina of diabetic mice [25]. Subsequent studies in our laboratory have revealed that, in addition to directly regulating vascular endothelial growth factor (VEGF), miR-200b can indirectly regulate VEGF through histone acetyltransferase p300 [25]. This action of miR-200b was repressed on exposure to high glucose, an effect also observed during incubation with TGF- $\beta$ 1 [26].

We have also reported that glucose-induced EndMT in the retina and heart of diabetic animals is regulated by miR-200b, through modulation of p300 [26, 27]. This was accompanied by the activation of TGF- $\beta$ -mediated Smad signalling and increased levels of ECM proteins [26, 27]. Although several miRNAs have been shown to inhibit EndMT through their actions on TGF- $\beta$ 1/Smad signalling, the only other miRNA known to regulate high glucose-induced EndMT is miR-142-3p [28]. Nevertheless, the role of lncRNAs in this milieu is currently less explored, and the role of H19 in EndMT during diabetic retinopathy remains unknown.

The purpose of this study was to decipher the role of H19 in EndMT development during diabetic retinopathy. We used human retinal microvascular endothelial cells (HRECs) to understand whether H19 regulates this phenomenon through TGF- $\beta$ -mediated Smad-dependent or Smad-independent pathways, and to elucidate the influence of H19 on miR-200b. We further expanded this study to include STZ-induced diabetes in mice and vitreous humour from diabetic individuals.

## Methods

All experimental groups were categorised based on their respective treatments (glucose or STZ-induction) and relevant controls. No randomisation was carried out. The researchers were not blinded to the experimental groups, unless otherwise mentioned.

**Cells** HRECs (Olaf Pharmaceuticals, Worcester, MA, USA; negative for mycoplasma; [www.interchim.fr/ft/E/EOC230.pdf](http://www.interchim.fr/ft/E/EOC230.pdf)) were grown in endothelial basal media-2 with 10% FBS [22] and plated at  $4.3 \times 10^5$  cells/ml. After 24 h of incubation with serum-free endothelial basal media-2, HRECs were treated with various concentrations of glucose (5 mmol/l, normal (D-) glucose [NG]; 25 mmol/l, high (D-) glucose [HG]) for 48 h. L-Glucose (25 mmol/l) was used as an osmotic control. Cells for transfection were seeded at  $7.5 \times 10^5$  cells/ml to achieve 90% confluency. HRECs were transfected with one of the following: silencer RNA, si*H19* (20 nmol/l; Dharmacon, Chicago, IL, USA), miRIDIAN miR-200b mimic or antagomir (20 nmol/l; Dharmacon) or overexpression vector pcDNA 3.1(+) vector harbouring a full-length cDNA sequence of human *H19* (NorClone Biotech Labs London, ON, Canada) using the transfection reagent Lipofectamine2000 (Invitrogen, Burlington, ON, Canada). Scrambled silencer RNA, miRIDIAN scrambled miR control or empty vector were used, respectively, as controls. Following transfection, cells were starved of serum for 24 h and treated with glucose as above. Each experiment was performed with three or more replicates and, unless specified, as previously reported with the removal of significant outliers that existed in data replicates [27].

**Animals** The mice were cared for based on guidance principles for the care and use of animals. Western University and Animal Care and Veterinary Services approved all the experiments, and these conformed to the *Guide for the care and use of laboratory animals* published by the National Institutes of Health (NIH; publication 85-23, revised 1996). All animals were monitored regularly during breeding, weaning, and pre- and post-treatment. Diabetic animals were regularly monitored for glucose levels, were provided with adequate food and water, and bedding was frequently changed because of frequent urination.

*H19<sup>Aex1</sup>* (also known as *H19<sup>tm1.1Sriv</sup>*) male mice, generated on a C57/BL6J background using a cre-loxP-based deletion strategy targeted to delete exon1 from *H19*, were used, along with C57/BL6J wild-type control animals [29]. The *H19<sup>Aex1</sup>* mice were a generous gift from K. Pfeifer (NIH, Bethesda, MD, USA). Blood glucose levels were measured in 8- to 10-week-old mice, and STZ was then administered intraperitoneally. The mice were given a total of five doses of STZ (50 mg/kg in citrate buffer, pH 5.6) on alternate days [30]. Sex- and age-matched littermate controls received an identical volume of citrate buffer. Hyperglycaemia (>20 mmol/l) was confirmed by measuring tail vein blood glucose using a glucometer. All treatment and control animals were frequently monitored and placed in metabolic cages (for 24 h) to collect urine after diabetes had been present for 8 weeks. Afterwards, all the mice were euthanised by a lethal dose of isoflurane and retinal tissues were collected. Major portions of the tissues were kept frozen, while small amounts were formalin-fixed and paraffin-embedded.

**Human vitreous humour** This part of the study was approved by the Western Research Ethics Board at Western University (London, ON, Canada). Informed consent was gained prior to procurement of the surgical samples, and all samples were handled according to the Declaration of Helsinki. Vitreous humour were collected from individuals undergoing a 25-gauge pars plana vitrectomy performed by an experienced vitreoretinal surgeon. Samples were categorised into groups of individuals diagnosed with proliferative diabetic retinopathy (PDR;  $n = 8$ , five men and three women; mean age  $\pm$  SD =  $76 \pm 3.77$  years) and non-diabetic individuals ( $n = 5$ , three men and two women; mean age  $\pm$  SD =  $61.6 \pm 8.35$  years) with no previous history of diabetes mellitus and diagnosed with an idiopathic macular hole or other non-diabetic ocular condition. All specimens were centrifuged at (12,000  $g$  for 10 min at  $4^{\circ}\text{C}$ ) and pellets were collected for RNA extraction [31, 32]. The pellets included fibrovascular tissue, hyalocytes and white blood cells [33, 34]. Vitreous humour samples showing haemorrhage were excluded to avoid contamination with RNA from blood cells.

**RNA analysis** Total RNA was extracted using TRIzol reagent (Invitrogen, Burlington, ON, Canada) [26]. cDNA for PCR was produced with a high-capacity cDNA reverse-transcription kit (Applied Biosystems, Burlington, ON, Canada). mRNA expression was measured using real-time RT-PCR using LightCycler (Roche Diagnostics, Mississauga, ON, Canada) and normalised to  $\beta$ -actin. Primers were designed with Primer 5 software (Premier Biosoft, Palo Alto, CA, USA; see electronic supplementary material [ESM] Table 1). The genes measured were human and mouse  $\beta$ -actin and *miR-200b*, *H19*, *CD31*, *VE-CAD* (also known as *CDH5*), *FSP1* (also known as *S100A4*), *SM22* (also known as *TAGLN*),  *$\alpha$ -SMA* (also known as *ACTA2*), *TGF- $\beta$*  (also known as *TGFB1*), *Cd31* (also known as *Pecam1*), *Ve-cad* (also known as *Cdh5*), *Fsp1* (also known as *S100a4*),  *$\alpha$ -Sma* (also known as *Acta2*) and *Vim*.

**miRNA analysis** The mirVana miRNA isolation kit (Ambion, Austin, TX, USA) was used to extract miRNA from HRECs. cDNA was synthesised using TaqMan microRNA Assay RT Primers and MultiScribe reverse transcriptase (Life Technologies, Burlington, ON, Canada) following the manufacturer's protocol [26]. TaqMan microRNA Assay was used to perform RT-qPCR in a LightCycler (Roche Diagnostics). Data were normalised to *U6* (also known as *RNU6-1*) small nuclear RNA.

**Fluorescence in situ hybridisation** As described [30, 35], cells were seeded at 75% confluency on glass cover slips in 12-well plates and treated with various concentrations of glucose for 48 h. Fluorescence in situ hybridisation (FISH) was performed according to the manufacturer's protocol (<https://www.biosearchtech.com/support/resources/stellaris-protocols>). The

human H19 probes were oligonucleotides tagged with CAL Fluor Red 610 Dye, mixed and pooled to a final concentration of 5 nmol (Biosearch Technologies, Petaluma, CA, USA). The HRECs hybridised with probes were counterstained with Hoechst 33342 (1 mg/ml; Invitrogen) and mounted with Vectashield mounting medium (Vector Labs, Burlingame, CA, USA). Images were captured with a fluorescent microscope (Olympus BX51; Olympus, Richmond Hill, ON, Canada) by researchers blinded to the experimental groups and analysed using ImageJ software (NIH, Bethesda, MD, USA).

**Immunofluorescence** HRECs were seeded on cover slips in 12-well plates at approximately 75% confluency. Following various treatments, cells were rinsed with PBS, fixed with methanol:acetone (4:1, vol./vol.) and permeated with 0.5% Triton X-100 in PBS [26]. After incubation with 5% normal serum, cells were incubated with one of the primary antibodies: mouse anti-CD31 (Abcam, Toronto, ON, Canada), rabbit anti-VE-cadherin (VE-cad; Santa Cruz, Dallas, TX, USA), rabbit anti-FSP1 (Abcam), rabbit anti-SM22 (Santa Cruz), goat anti-vimentin (Santa Cruz) and rabbit anti-TGF- $\beta$  (Abcam) at 1:100 dilutions as previously described [26]. Secondary antibodies conjugated with Alexa Fluor 488 (goat anti-mouse IgG, goat anti-rabbit IgG or donkey anti-goat IgG [Invitrogen]) were used at 1:200 dilutions. A fluorescent microscope (Olympus BX51) was used for image capture by researchers blinded to the experimental groups, and images were analysed with ImageJ software. Hoechst 33342 was used as a nuclear stain.

**Immunohistochemical analyses for permeability** Paraffin-embedded retinal tissues were immunocytochemically stained for IgG using anti-mouse IgG antibody (MP Biomedicals, Solon, OH, USA) [30, 32]. All stains were arbitrarily scored (0–3) in a masked fashion.

**Western blotting** HRECs overexpressing *H19* vector and control samples were exposed to NG and HG conditions for 48 h. Total proteins were extracted with RIPA buffer (Thermo Fisher, Markham, ON, Canada) containing protease inhibitor (cOmplete Mini Tablet; Roche). A bicinchoninic acid protein assay kit (Pierce, Rockford, IL, USA) was used to determine protein concentration. A total of 30  $\mu\text{g}$  of protein was resolved by 10% SDS gel electrophoresis, transferred to a polyvinylidene difluoride membrane (Bio-Rad, Hercules, CA, USA) and incubated overnight at  $4^{\circ}\text{C}$  with one of the primary antibodies: mouse anti-CD31, rabbit anti-FSP1 (1:1000 and 1:100, respectively; Abcam); rabbit anti-SM22, mouse anti- $\beta$ -actin antibody (1:200 and 1:400, respectively; Santa Cruz); rabbit anti-p-ERK1/2, rabbit anti-ERK1/2, rabbit anti-p-Smad2/3, mouse anti-Smad2/3 (1:1000; Cell Signaling Technology, Beverly, MA, USA); polyclonal anti-Akt and anti-p-Akt (Ser473 and Thr308) (1:1000; New England

BioLabs, Pickering, ON, Canada). The membranes were then incubated with HRP-conjugated anti-rabbit antibody (1:10,000; Upstate Biotechnology, Charlottesville, VA, USA) or anti-mouse antibody (1:10,000; Vector Laboratories) for 1 h at room temperature [36]. All antibodies were diluted in Tris-buffered saline–tween (TBST) (25 mol/l Tris base, 150 mol/l NaCl, 3 mol/l KCl, 0.1% Tween 20), pH adjusted to 7.4–7.6. Blots were visualised using electrochemiluminescence (Amersham Pharmacia Biotechnology, Amersham, UK). Quantification of blots was performed by densitometry using Mocha software (SPSS, Chicago, IL, USA) and all blots were taken from the respective membranes and cropped to improve clarity. As noted in the product protocols, all antibodies were validated by the manufacturer.

**Luminex assay** Components of TGF- $\beta$  signalling were measured using the Milliplex MAP TGF- $\beta$  signalling pathway magnetic bead 6-plex-Cell Signaling Multiplex assay (Millipore, Burlington, MA, USA). The kit comprised p-Akt (Ser473), p-ERK1/2 (Thr185/Tyr187), p-Smad 2 (Ser465/Ser467), p-Smad3 (Ser423/Ser425), Smad4 (total) and TGF- $\beta$  receptor II (TGF $\beta$ RII) (total) analytes. The manufacturer's protocol was followed, and total protein from the extracted lysate was measured using bicinchoninic acid. Samples (<500 mg/ml) were assessed using Luminex technology with a Milliplex MAP TGF- $\beta$  signalling kit containing a multiplex magnetic bead-based antibody detection kit [30].

**Statistical analysis** The statistical significance was determined by Student's *t* test (unpaired) or one-way ANOVA followed by a post hoc test when appropriate. Data were expressed as mean  $\pm$  SD, and a *p* value of 0.05 or less was considered significant. All results are expressed as the mean of *n* = 5–7 per group. GraphPad Prism 5 software (GraphPad, La Jolla, CA, USA) was used for statistical analysis.

## Results

**H19 expression is regulated in endothelial cells by exposure to glucose** Our first aim was to study the alterations in H19 in HRECs after glucose exposure. We had previously performed a microarray analysis on HRECs exposed to HG for 48 h to study expression levels of lncRNAs [30]. Array results showed one of the highest levels of downregulation of H19 with HG compared with NG treatment (Gene Expression Omnibus [GEO] accession number GSE122189). Furthermore, duration-dependent analyses of H19 expression showed one of its lowest levels after 48 h of HG exposure and no changes in concentration with 25 mmol/l L-glucose. We validated glucose-mediated downregulation of H19 expression in these HRECs by measuring H19 RNA expression after HG treatment (an approximately 50% reduction, *p* < 0.0243)

(Fig. 1a). Cellular H19 expression was visualised by RNA FISH, which helped us delineate its subcellular distribution. FISH analyses showed significant reductions in H19 expression in HG-treated cells (Fig. 1b,c). In the control groups (NG), H19 was distributed partly in the nucleus but predominantly in cytoplasm. When treated with HG, although both nuclear and cytoplasmic positivity were reduced, the changes were pronounced in the nucleus. To examine whether this finding was clinically relevant, we performed similar analyses in the vitreous humour samples. H19 RNA expression levels were significantly lower in the diabetic vitreous humour vs controls (Fig. 1d).

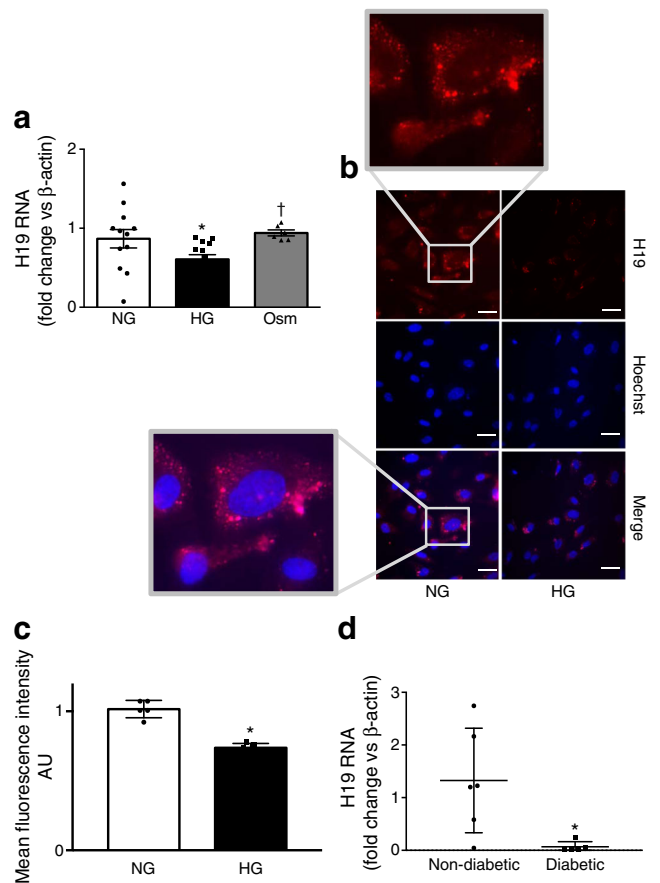


**Fig. 1** H19 expression in glucose-treated HRECs. **(a)** H19 RNA expression measured using real-time RT-PCR was reduced on exposure to 25 mmol/l D-glucose (HG, 48 h), but there was no difference between 5 mmol/l D-glucose (NG) control cells and cells exposed to 25 mmol/l L-glucose as an osmotic control (Osm, 48 h). **(b)** FISH using human H19 probes showed a decrease in H19 expression in HRECs exposed to HG conditions, with largely cytoplasmic localisation in comparison to NG. **(c)** Quantification of FISH data performed using ImageJ confirmed glucose-induced H19 downregulation in terms of mean fluorescence intensity; AU, arbitrary units. **(d)** RNA analysis (mean  $\pm$  SD) of vitreous humour in diabetic participants indicated a decrease in H19 levels compared with non-diabetic individuals. Scale bars, 10  $\mu$ m. RNA data are expressed as a ratio to  $\beta$ -actin, normalised to control. Data are mean  $\pm$  SD; \**p* < 0.05 vs NG or non-diabetic participants; †*p* < 0.05 vs HG. *n* = 6 per group

**H19 reverses glucose-mediated EndMT in HRECs and in retinas in diabetes** EndMT is characterised by a decrease in the expression of endothelial markers and gain of a more mesenchymal phenotype. We employed multiple markers to validate this transition. For the endothelial markers, we used CD31 and VE-cad, while the mesenchymal markers used were FSP1, SM22,  $\alpha$ -SMA and vimentin—representing well-characterised EndMT markers [26, 27]. Based on our previous duration-dependent analyses [26, 27, 30] and from the well-established work of other investigators [37, 38], we found that glucose-induced changes in several molecules occurred at the 48 h mark; we therefore used this time point for our in vitro experiments. HG treatment produced a significant downregulation of the endothelial markers *CD31* (also known as *PECAMI1*) and *VE-CAD* (Fig. 2a,b), accompanied by an upregulation of mesenchymal markers *FSP1*, *SM22* and  $\alpha$ -*SMA* (Fig. 2c–e). As the expression of H19 was reduced in HG-exposed HRECs, we overexpressed H19 to establish a cause-

and-effect relationship. We used a pcDNA 3.1(+) vector harbouring a full-length cDNA sequence of human *H19*. We transfected HRECs with an empty vector (control) or *H19*-pcDNA 3.1, followed by treatment with varying concentrations of glucose. We then quantified mRNA levels. Overexpression of H19 reversed EndMT markers in spite of the HG environment (Fig. 2a–e), indicating that glucose-induced EndMT changes are mediated through H19 in HRECs. As miR-200b is a well-known negative regulator of EndMT [26, 27], we conducted a similar experiment with miR-200b mimic transfection followed by HG incubation, confirming its prevention of HG-induced EndMT (Fig. 2a–e).

To identify a relationship of H19 with miR-200b in this context, we performed additional experiments (Fig. 2a–e). H19 overexpression increased basal and glucose-induced miR-200b downregulation, while silencing of H19 had a reverse effect, indicating H19 as a positive regulator of miR-200b (Fig. 2f,g). However, H19 expression was unaffected by miR-200b

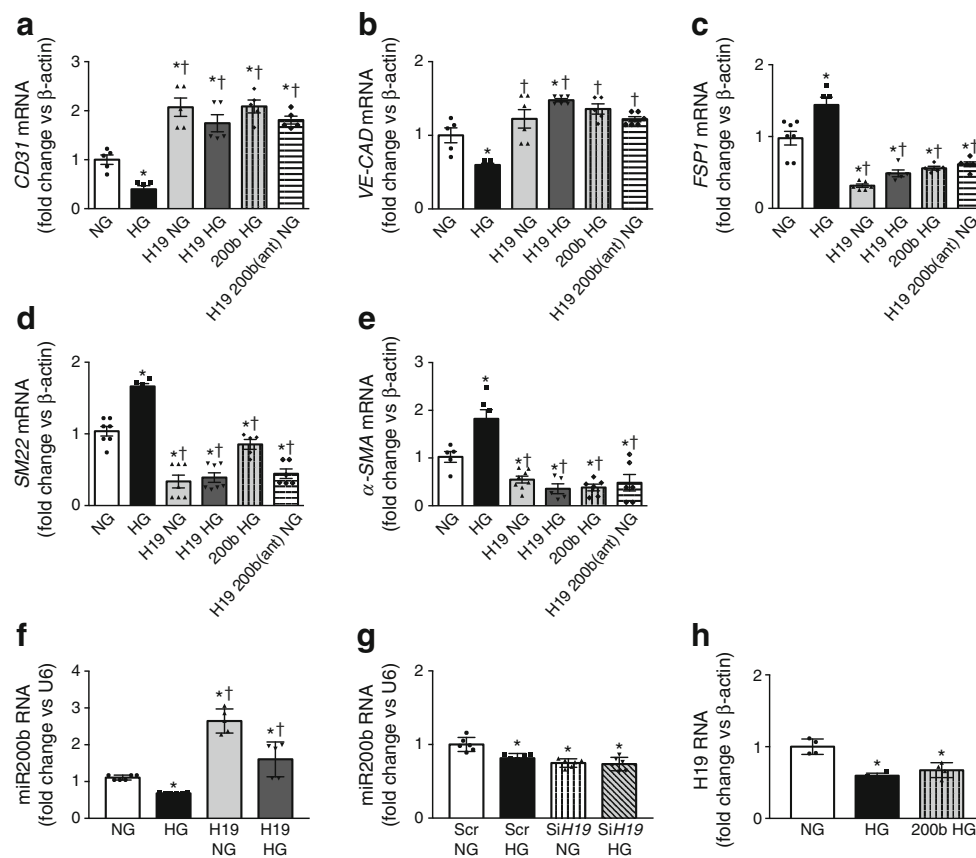


**Fig. 2** Effect of H19 overexpression on EndMT markers at the mRNA level in HRECs. (a–f) Treatment of HRECs with HG reduced the mRNA expression of endothelial markers *CD31* (a) and *VE-CAD* (b), and increased the expression of mesenchymal markers *FSP1* (c), *SM22* (d) and  $\alpha$ -*SMA* (e), compared with NG. Overexpression of H19 (H19 NG and H19 HG) reversed these alterations in EndMT markers, and similarly miR-200b overexpression (using miR-200b mimics [200b HG]) corrected the HG-induced alteration of EndMT markers (a–e). H19 overexpression increased basal and glucose-induced downregulation of miR-

200b (f) and rescued cells from EndMT in spite of a blockade of miR-200b using antagonists [H19 200b(ant) NG] (a–e). (g) H19 siRNA transfection (*siH19*) had a glucose-like effect on miR-200b. (h) H19 levels were unaffected by overexpression of miR-200b under HG conditions. mRNA/RNA data are expressed as a ratio to  $\beta$ -actin; miRNA data are expressed as a ratio to U6 normalised to control; mean  $\pm$  SD. \* $p$ <0.05 vs empty vector treated with NG; † $p$ <0.05 vs empty vector treated with HG.  $n=5$  per group

overexpression in an HG environment, indicating that miR-200b was unable to reverse HG-induced decreases in H19 (Fig. 2h). In order to further delineate a direct relationship, we performed a rescue experiment. We used miR-200b antagonists in an NG environment and then overexpressed H19. Such an intervention prevented glucose-induced EndMT. These findings suggest that, under HG conditions, H19 is not regulated by miR-200b and may be working independently (Fig. 2a–e).

We extended our study to confirm EndMT changes at a protein level. In all instances, HG-induced reductions in endothelial markers were corrected with H19 overexpression (Fig. 3a–d). Furthermore, the HG-induced increase in mesenchymal markers was also corrected following H19 overexpression (Fig. 4a–d, ESM Fig. 1), in keeping with the mRNA levels. Immunofluorescent studies were accompanied by western blotting that confirmed H19-induced overexpression of CD31 and

downregulation of SM22 and FSP1, compared with the HG control (Fig. 5a–c).

siRNA-mediated silencing in NG produced a glucose-like effect on EndMT markers. Interestingly, lowering of H19 expression in an HG environment had no further effects on these markers, suggesting that such alterations had already reached their lowest levels following HG incubation (Fig. 6a–e). In animal experiments, diabetic wild-type and *H19*<sup>Δex1</sup> mice, along with their control animals, were monitored for 2 months. This time point was selected as we are able to maintain diabetic mice for up to 2 months without exogenous insulin. Furthermore, we and several groups have demonstrated that early and functional changes of diabetic retinopathy develop at this time point [30, 32, 39]. Elevated blood glucose, polyuria and reduced body weight were evident in diabetic animals, indicative of poorly controlled diabetes (ESM Table 2).

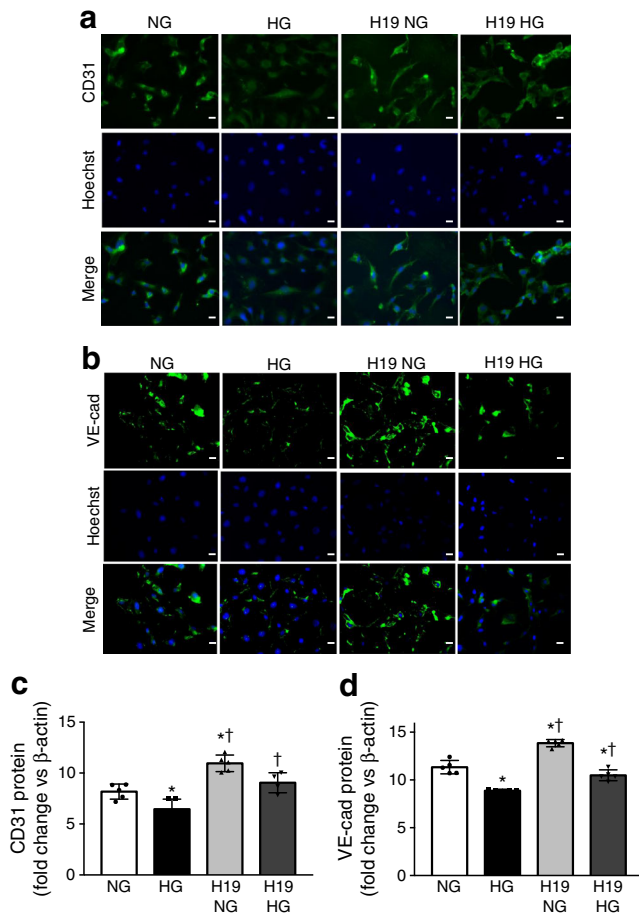


**Fig. 3** Effect of H19 upregulation on protein expression of endothelial markers. Immunofluorescence staining of HREC cells showed reduced production of endothelial markers CD31 (a) and VE-cad (b) in HG vs NG. These alterations were prevented in H19-overexpressing HREC cells (H19 NG and H19 HG). Quantification data using ImageJ confirmed these findings (c, d). Scale bars, 10 μm. Protein data are expressed as a ratio to β-actin, normalised to control (mean ± SD); \* $p < 0.05$  vs empty vector treated with NG; † $p < 0.05$  vs empty vector treated with HG.  $n = 5$  per group

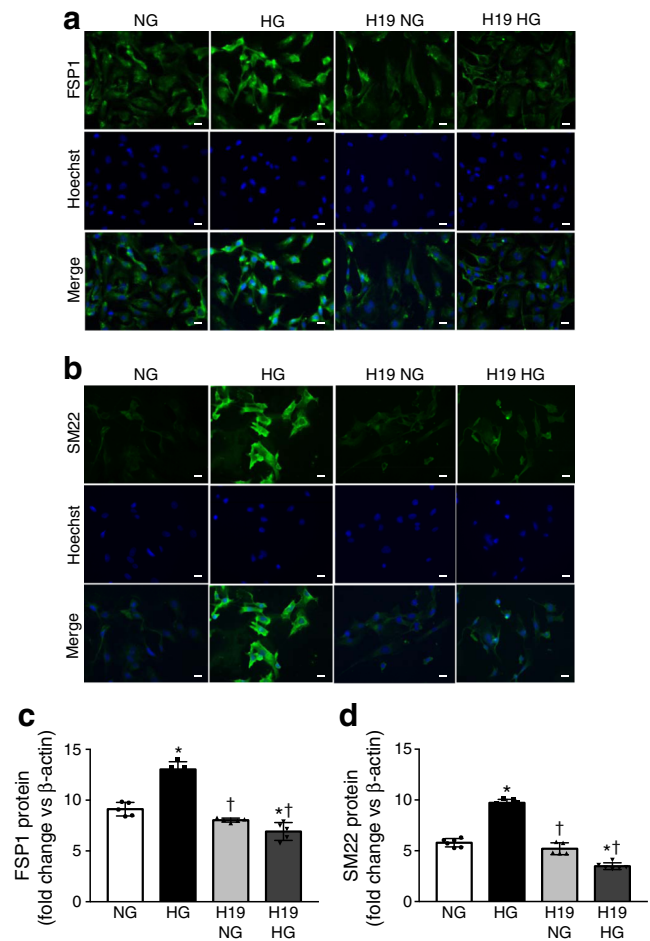


**Fig. 4** Effect of H19 on mesenchymal markers at the protein level. Immunofluorescence staining of HREC cells showed increased production of mesenchymal markers FSP1 (a) and SM22 (b) in cells treated with HG vs NG. H19 overexpression (H19 NG and H19 HG) downregulated these markers in HREC cells. Quantification data using ImageJ confirmed the findings (c, d). Scale bars, 10 μm. Protein data are expressed as a ratio to β-actin normalised to control (mean ± SD). \* $p < 0.05$  vs empty vector treated with NG; † $p < 0.05$  vs empty vector treated with HG.  $n = 5$  per group

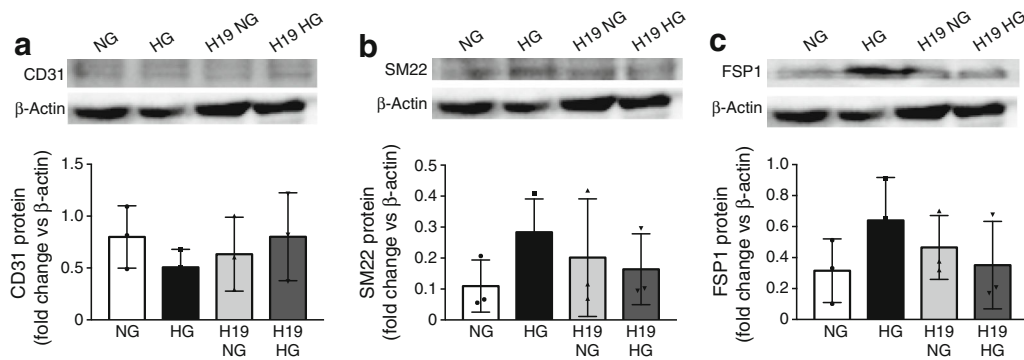


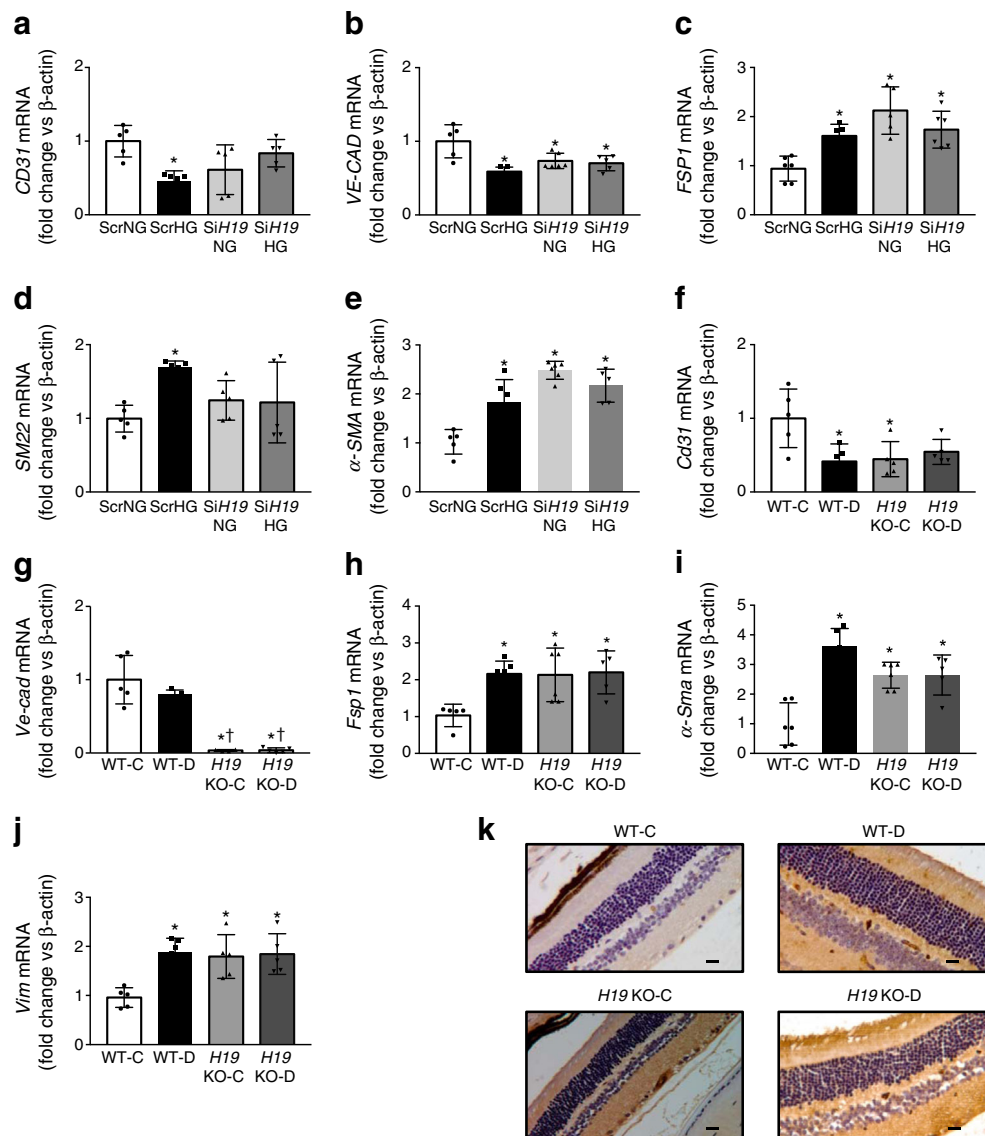
**Fig. 5** Western blots confirm that H19 overexpression prevents EndMT. Treatment with HG reduced protein levels of endothelial markers CD31 (a) and increased levels of mesenchymal markers SM22 and FSP1 (b, c) compared with NG in HRECs. Transfection with H19-overexpressing

vector (H19 NG and H19 HG) prevented such changes. Representative western blots and densitometric analyses (mean  $\pm$  SD) are shown.  $n=3$  per group. Protein data are expressed as a ratio to  $\beta$ -actin

Animal retinal tissues showed diabetes-induced reductions in H19 along with retinal changes of EndMT: reduced endothelial

and increased mesenchymal markers. Such changes were also observed in *H19* knockout (KO) mice (Fig. 6f–j). Retinal

**Fig. 6** *H19* siRNA transfection led to a glucose-like EndMT phenotype. (a–e) *H19* siRNA transfection of HRECs reduced endothelial markers *CD31* (a) and *VE-CAD* (b), and upregulated mesenchymal markers *FSP1* (c), *SM22* (d) and  $\alpha$ -*SMA* (e) in NG. No further enhancement of EndMT was seen when similar transfection was carried out in HG. (f–j) Similarly, *H19*<sup>Δex1</sup> mice (*H19* KO-C) demonstrated a diabetes-like EndMT phenotype in the retina. No further exaggeration of EndMT was seen when diabetes was induced in the KO animals (*H19* KO-D). (k) Immunohistochemical staining of the mouse retina for IgG showed enhanced extravascular diffuse stain, signifying increased extravasation in the wild-type diabetic (WT-D; score 3), *H19* KO-C (score 2) and *H19* KO-D (score 3) mice compared with wild-type controls (WT-C; score 0). Scale bars, 10  $\mu$ m. mRNA data (mean  $\pm$  SD) are expressed as a ratio to  $\beta$ -actin, normalised to control. \* $p<0.05$  vs scrambled siRNA in NG (ScrNG); † $p<0.05$  vs wild-type control (WT-C).  $n=6$  per group





tissues were stained for IgG, as IgG extravasation is a marker of increased vessel permeability [30, 32]. Wild-type diabetic and *H19* KO diabetic animals showed an increase in vascular leakage (a score of 3, compared with a score of 0 in wild-type control animals, and a score of 2 in *H19* KO control animals; Fig. 6k).

**H19 regulates TGF- $\beta$  to suppress EndMT** As TGF- $\beta$  is an important regulator of EndMT [26], we examined whether H19 was regulating TGF- $\beta$ 1 levels. H19 overexpression inhibited TGF- $\beta$ 1 and prevented glucose-mediated TGF- $\beta$ 1 upregulation at both the mRNA (Fig. 7a) and protein (Fig. 7b,c) levels. The effect of H19 was not influenced by the varying levels of glucose. Since miR-200b regulates EndMT through TGF- $\beta$ 1 [26], we also confirmed miR-200b-mediated regulation of EndMT using miR-200b mimic transfection followed by HG incubation (Fig. 7a). To understand whether the regulation of TGF- $\beta$ 1 by H19 was dependent on miR-200b, we performed a rescue experiment in which we suppressed miR-200b expression using miR-200b antagonists in NG and then overexpressed H19. The TGF- $\beta$ 1 levels continued to be downregulated, further indicating possible H19 action independent of miR-200b (Fig. 7a).

**H19 regulates TGF- $\beta$ 1-mediated EndMT through a Smad-independent MAPK-ERK1/2 pathway** To identify TGF- $\beta$  signalling pathway candidates affected by H19's regulation of

EndMT, we used Luminex technology. We performed the experiments in endothelial cells as doing such specific signalling analyses on the whole tissue might not have provided a clear answer. Luminex assay permitted simultaneous relative quantification of several phosphorylated and total TGF- $\beta$  signalling proteins from cell lysates. HG caused increased production or phosphorylation of TGF $\beta$ RII (total), p-Smad 2, p-Smad 3 and Smad 4 (total), p-Akt and p-ERK1/2 proteins (Fig. 8a–f). HREC cells were also transfected with *H19*-pcDNA 3.1 vector and treated with NG (H19 NG) and HG (H19 HG). TGF $\beta$ RII (total) was significantly reduced following H19 overexpression (Fig. 8a). Basal levels of Smad proteins (p-Smad 2, p-Smad 3, Smad 4) and p-Akt were increased following H19 overexpression (Fig. 8b–e). However, levels of these molecules in the HG environment appeared to be unaltered following H19 overexpression. Interestingly, p-ERK1/2 levels were significantly downregulated in samples overexpressing H19 irrespective of the influence of glucose in these groups (Fig. 8f). We confirmed these results of p-Smad 2/3 and p-Akt proteins by western blotting (Fig. 8g,h). p-ERK1/2 protein levels were significantly downregulated after H19 overexpression, similar to the Luminex assay (Fig. 8i). This led us to conclude that H19 suppresses glucose-mediated EndMT through regulation of the MAPK-ERK1/2 pathway of TGF- $\beta$  signalling using a Smad-independent route (Fig. 9).

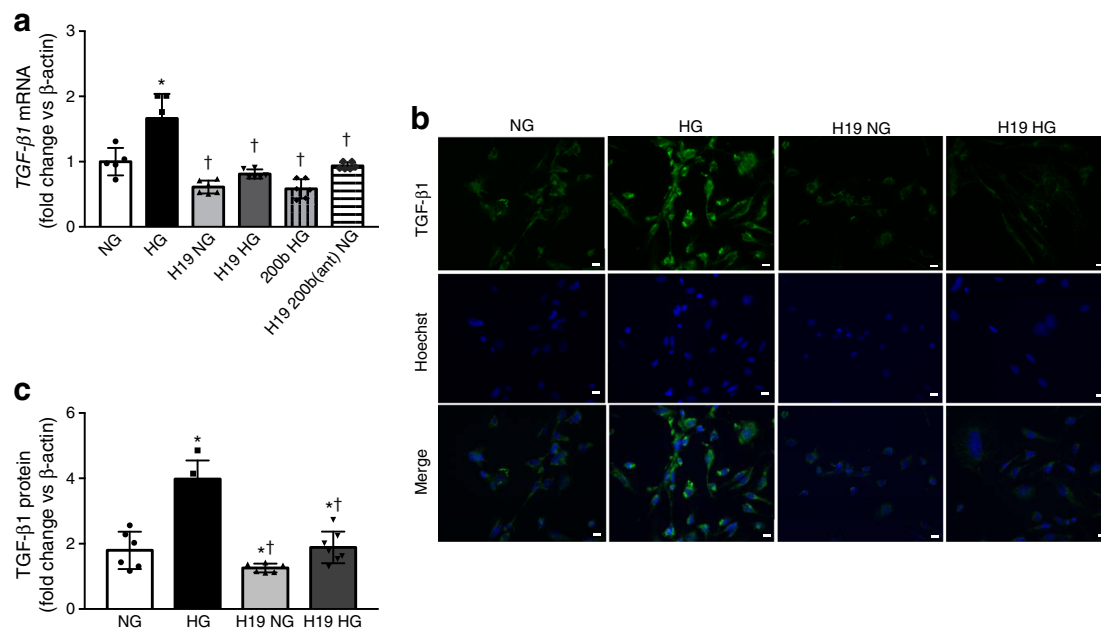
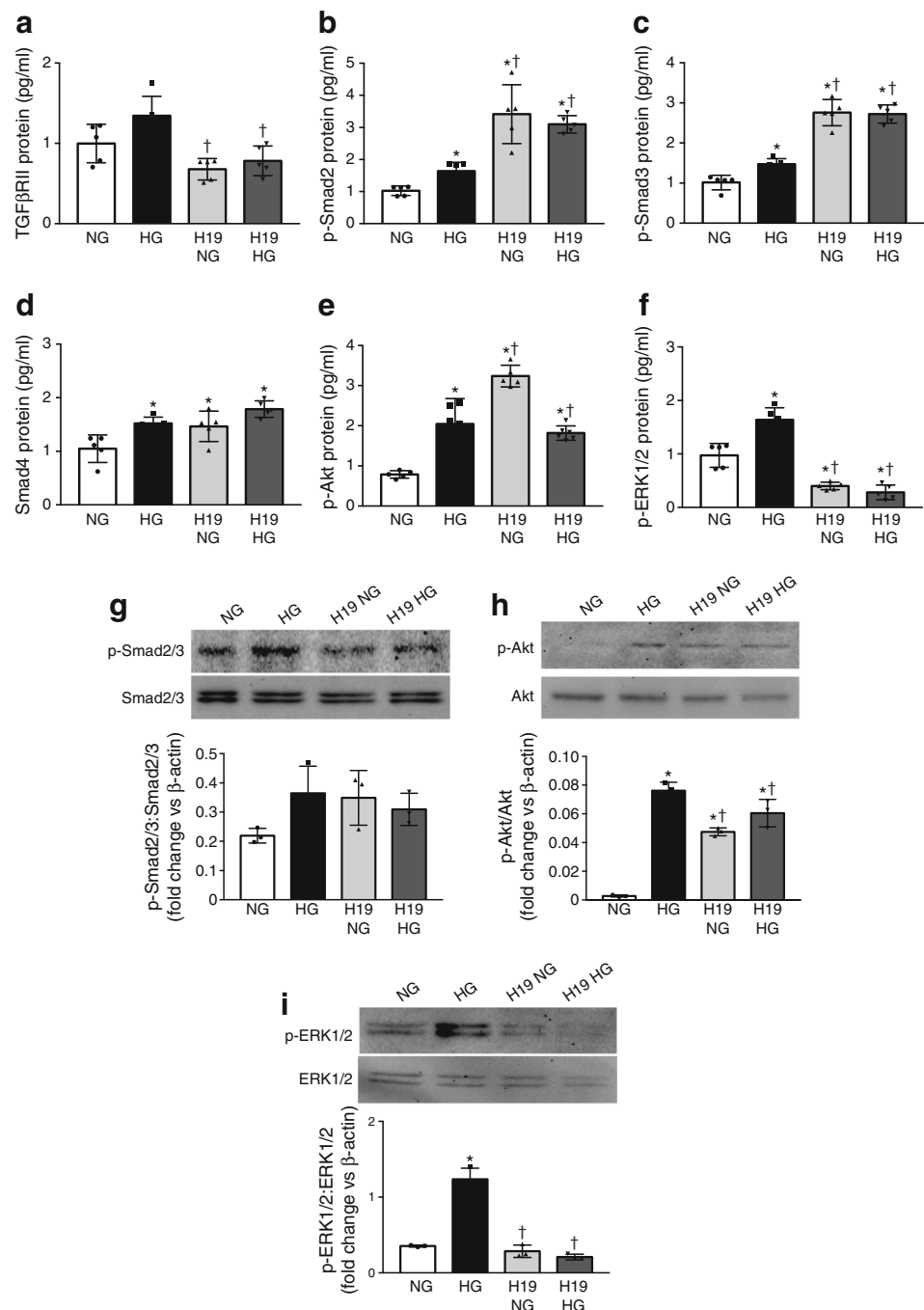


**Fig. 7** H19 prevents glucose-mediated upregulation of TGF- $\beta$ 1. (a) HG treatment in HRECs increased mRNA expression of *TGF- $\beta$ 1* compared with NG. H19 overexpression (H19 NG and H19 HG) reduced *TGF- $\beta$ 1* in both the NG and HG environments. A similar reduction was seen following miR-200b mimic transfection (200b HG). miR-200b antagonists [H19 200b(ant) NG] failed to rescue H19 overexpression-induced *TGF- $\beta$ 1* downregulation. (b, c) Exposure to HG elevated TGF-

$\beta$ 1 protein levels in HRECs. H19 overexpression downregulated the increase in TGF- $\beta$ 1 protein on exposure to varying glucose levels (H19 NG and H19 HG). Quantification data using ImageJ confirmed the findings (c). Scale bars, 10  $\mu$ m. mRNA and protein levels were expressed as a ratio to  $\beta$ -actin (mean  $\pm$  SD). \* $p$ <0.05 vs empty vector treated with NG; † $p$ <0.05 vs empty vector treated with HG.  $n$ =5 per group

**Fig. 8** H19 regulates EndMT through a Smad-independent MAPK–ERK1/2 pathway. (a–f) A Luminex assay panel for TGF- $\beta$  signalling was used to quantify several proteins: TGF $\beta$ RII (total), p-Smad2, p-Smad3, Smad4 (total), p-Akt and p-ERK1/2. These proteins were upregulated in HRECs when exposed to HG treatment compared with NG. H19 overexpression downregulated the increase in TGF $\beta$ RII (total), in both NG and HG conditions (a). Increased H19 levels did not reduce p-Smad2 (b), p-Smad3 (c), Smad4 (total) (d) or p-Akt (e) protein levels. p-ERK1/2 protein levels were significantly downregulated (f) as a result of H19 overexpression in HRECs with NG and HG treatments. (g–i) Representative western blots and densitometric analyses of (g) p-Smad2/3:Smad2/3 show no effect following H19 overexpression. (h) p-Akt protein expression was slightly reduced by H19 overexpression. (i) Glucose-induced increases in p-ERK1/2 significantly decreased following H19 overexpression. Protein levels are expressed as a ratio to  $\beta$ -actin (mean  $\pm$  SD); \* $p$ <0.05 vs empty vector treated with NG; † $p$ <0.05 vs empty vector treated with HG.  $n$ =6 per group except for western blots, which were  $n$ =3 per group



## Discussion

Our current study deciphers the role of lncRNA H19 in diabetes-induced EndMT in HRECs. We report that H19 overexpression prevents glucose-induced EndMT through TGF- $\beta$ 1 and subsequent TGF- $\beta$  signalling via a blockade of the MAPK–ERK1/2 pathway. To demonstrate these changes, we conducted experiments using H19 overexpression vector and H19-silencing siRNA in HRECs. Furthermore, such regulatory action of H19 occurs independently of miR-200b, a

miRNA previously shown to regulate diabetes-induced EndMT [26, 27]. Our animal experiments confirmed the role of H19 in retinal EndMT, and the human vitreous humour findings showed hyperglycaemia-induced downregulation of H19 in PDR compared with non-diabetic individuals.

lncRNAs play important roles in cancer metastasis through regulation of EMT by targeting multiple signalling pathways including TGF- $\beta$  signalling [40]. The lncRNA *MALAT1* can modulate TGF- $\beta$ 1-induced EndMT in isolated endothelial progenitor cells by negatively regulating miR-145 [41]. Another

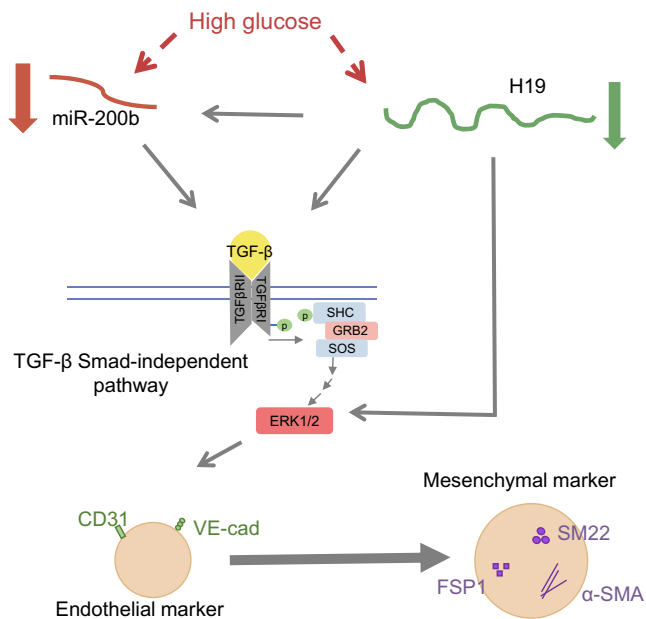


**Fig. 9** An overview of the various processes described in the study. H19 is downregulated under high glucose conditions and regulates the expression of miR-200b. H19 and miR-200b regulate TGF- $\beta$ 1 signalling. Overexpression of H19 decreases TGF- $\beta$ 1 levels and affects the TGF- $\beta$ 1–MAPK–ERK1/2 signalling pathway (a Smad-independent pathway [SHC–transforming protein, GRB2, SOS]) by preventing pERK1/2 protein expression. In turn, this leads to an increase in endothelial markers and a reduction in mesenchymal markers, leading to prevention of EndMT. GRB2, growth factor receptor-bound protein 2; SHC, Src homology 2 domain-containing; SOS, son of sevenless protein

study has revealed that hypoxia-induced EndMT in human umbilical vein endothelial cells was promoted by the lncRNA *GATA6-AS*, through histone methylation [42]. Nevertheless, the role of lncRNAs in regulating hyperglycaemia-induced EndMT remains unclear. We have reported here for the first time a regulatory role of lncRNA H19 in glucose-mediated EndMT through its inhibition of TGF- $\beta$ 1 and its subsequent signalling pathway. H19 has been well studied in tumours, but its role in diabetic complications is not certain. Our data are similar to those of a previous study reporting downregulation of H19 in cardiac tissues of diabetic rats [24]. Our FISH analyses also revealed that although H19 was distributed across the cell cytoplasm and nucleus in normal cells, high glucose treatment reduced its expression to a few scattered spots predominately in the cytoplasm [23]. The exact reasons for such subcellular changes need further exploration. Moreover, during EMT in cancers, TGF- $\beta$  is an important inducer of H19 through activation of the PI3K/Akt signalling pathway [43]. However, in our study, H19 suppressed TGF- $\beta$ 1 and TGF- $\beta$ IIIR during EndMT in HRECs. Overexpression of H19 significantly reduced TGF- $\beta$ 1 levels, resulting in the prevention of EndMT in spite of high glucose conditions. Such findings suggest alternative epigenetic regulatory mechanisms of H19 that require further studies.

Hyperglycaemia is the central event leading to micro- and macrovascular pathologies in diabetes [44]. Endothelial cells are exposed to circulating blood glucose and are the primary cell type to be affected by hyperglycaemia [44–46]. Endothelial cell dysfunction ensues as endothelial cells lose their quiescence, elude their normal function and acquire new phenotypes [32, 45]. Evidence suggests that endothelial cells then acquire a mesenchymal phenotype and begin to express markers characteristic of myofibroblasts, contributing to the advancement of sclerotic diseases [47, 48]. In PDR, fibrotic and inflammatory alterations in the epiretinal membranes are characterised by  $\alpha$ -SMA-expressing myofibroblasts and inflammatory cells in the stromal compartment [49]. We and others have reported the development of hyperglycaemia-induced EndMT in diabetic complications [26, 27, 50]. In this study, EndMT was reproduced in HRECs as we observed decreased endothelial markers CD31 and VE-cad, and increased mesenchymal markers FSP1, SM22,  $\alpha$ -SMA and vimentin. Furthermore, our animal data demonstrated similar changes in the retina of diabetic animals, which were further pronounced following *H19* KO. IgG staining revealed enhanced vascular permeability in wild-type and *H19* KO diabetic animals compared with wild-type controls. In addition, vitreous humour from participants with PDR showed downregulation of H19.

EndMT was originally identified as an embryonic mechanism for cardiac valve development from endothelial cells of the atrioventricular canal [51]. It is also involved in angiogenic sprouting in the postnatal retina, causing mesenchymal cells to be formed at the tips of vascular sprouts mediated by VEGF-A [52]. EndMT has recently emerged as a major contributor to various pathologies such as organ fibrosis [26, 27, 53, 54]. EndMT is also suggested to influence the development of fibroblasts and myofibroblasts, which are responsible for the progression of fibrosis and advancement of PDR [48]. A number of EndMT-inducing stimuli have been identified, including growth factors, cell–cell interactions, shear stress, environmental factors (e.g. hypoxia and hyperglycaemia) and, recently, epigenetics [55, 56]. Epigenetic modifications have been shown to contribute to EndMT, which is a stable alteration in cell phenotype [56]. Aberrant promoter methylation [56], histone deacetylase 3-mediated repression [57] and several miRNAs [58] are regulators of EndMT. Our previous work has also reported miR-200b as a negative regulator of diabetes-induced EndMT in retinal and cardiac cells and tissues [26, 27]. Data from the current study, however, suggest that H19 may influence EndMT independently of miR-200b. This proposed pathway requires further characterisation.

TGF- $\beta$  is described as the major regulator of EndMT and harbours profibrotic properties by inducing and propagating resident fibroblasts [59]. As TGF- $\beta$ 1 mediates both Smad-

dependent and Smad-independent pathways, we investigated whether these pathways were regulated by H19. Our previous work on epigenetic regulation of EndMT in diabetic retinopathy describes a Smad-dependent regulation of TGF- $\beta$ 1 mediated by miR-200b and histone acetyltransferase p300 [26]. We employed the Luminex assay that quantified phosphorylated proteins of Smad-dependent (p-Smad2 and p-Smad3) and Smad-independent (p-Akt and p-ERK1/2) pathways. The analysis showed no effect on Smad proteins and p-Akt levels following overexpression of H19. Conversely, H19 regulated the production of phosphorylated ERK1/2 proteins, suggesting that H19-mediated suppression of EndMT occurs through a Smad-independent pathway. Although we confirmed these results by western blotting, we recognise the need for extended study into the mechanisms involved in such regulation.

In conclusion, our data describes a novel role of lncRNA H19 in regulating EndMT induced by elevated glucose levels. H19 facilitates this regulation by suppressing TGF- $\beta$ 1 and its signalling pathways by repressing the MAPK-ERK1/2 signalling pathway. A schematic diagram of such a regulatory process is outlined in Fig. 9. We recognise that additional mechanisms may be in place to regulate such pathways, which warrants further exploration. Nevertheless, our findings open up possibilities for RNA-based therapies targeting a fundamental glucose-mediated cellular phenotypic alteration.

**Acknowledgements** We sincerely thank K. Pfeifer and his team from the National Institutes of Health (NIH) Intramural Research Program, Bethesda, MD, USA, for providing us with *H19<sup>Aex1</sup>* mice. Parts of this study were presented in abstract form at the 2017 Canadian Society of Endocrinology and Metabolism/Diabetes Canada Professional Conference and Annual Meeting, Edmonton, AB, Canada, 1–4 November 2017.

**Data availability** All data generated or analysed during this study are included in this published article (and its ESM). Nevertheless, the results from our lncRNA microarray can be found in GEO (<https://www.ncbi.nlm.nih.gov/geo/>) using the accession number GSE122189.

**Funding** This work was supported by grants from the Heart and Stroke Foundation of Ontario (HSF-G-16-00012556) and the Canadian Diabetes Association (CDA-OG-3-07-2380-SC) awarded to SC.

**Duality of interest** The authors declare that there is no duality of interest associated with this manuscript.

**Contribution statement** AAT, SB, BF, SChe, JG and SCha contributed to the study concept and design, performance of the experiments, data review and analysis, and writing and editing of the manuscript. All authors contributed to the critical revision of the manuscript and gave their final approval of the submitted version. SCha is the guarantor of this work and, as such, had full access to all the data in the study and takes responsibility for the integrity of the data and the accuracy of the data analysis.

**Publisher's note** Springer Nature remains neutral with regard to jurisdictional claims in published maps and institutional affiliations.

## References

- Guariguata L, Whiting DR, Hambleton I, Beagley J, Linnenkamp U, Shaw JE (2014) Global estimates of diabetes prevalence for 2013 and projections for 2035. *Diabetes Res Clin Pract* 103(2): 137–149. <https://doi.org/10.1016/j.diabres.2013.11.002>
- Fowler MJ (2008) Microvascular and macrovascular complications of diabetes. *Clin Diab* 26(2):77–82. <https://doi.org/10.2337/diaclin.26.2.77>
- Yau JW, Rogers SL, Kawasaki R et al (2012) Global prevalence and major risk factors of diabetic retinopathy. *Diabetes Care* 35(3):556–564. <https://doi.org/10.2337/dc11-1909>
- Wong TY, Cheung CM, Larsen M, Sharma S, Simó R (2016) Diabetic retinopathy. *Nat Rev Dis Primers* 2:1–16
- Balakumar P, Jindal S, Shah DI, Singh M (2007) Experimental models for vascular endothelial dysfunction. *Trends Med Res* 2: 12–20
- Ceriello A (2010) Postprandial glucose levels are a clinically important treatment target. *Diabetes Care* 33(8):1905–1907. <https://doi.org/10.2337/dc10-0634>
- Hadi HAR, Suwaidi JA (2007) Endothelial dysfunction in diabetes mellitus. *Vasc Health Risk Manag* 3(6):853–876
- Karsdal MA, Manon-Jensen T, Genovese F et al (2015) Novel insights into the function and dynamics of extracellular matrix in liver fibrosis. *Am J Physiol Gastrointest Liver Physiol* 308(10): G807–G830. <https://doi.org/10.1152/ajpgi.00447.2014>
- Wynn TA (2007) Common and unique mechanisms regulate fibrosis in various fibroproliferative diseases. *J Clin Invest* 117(3): 524–529. <https://doi.org/10.1172/JCI31487>
- Ho YY, Lagares D, Tager AM, Kapoor M (2014) Fibrosis—a lethal component of systemic sclerosis. *Nat Rev Rheumatol* 10(7):390–402. <https://doi.org/10.1038/nrrheum.2014.53>
- Lin F, Wang N, Zhang T (2012) The role of endothelial-mesenchymal transition in development and pathological process. *Life* 64(9):717–723. <https://doi.org/10.1002/iub.1059>
- Ohta S, Suzuki K, Tachibana K, Tanaka H, Yamada G (2007) Cessation of gastrulation is mediated by suppression of epithelial-mesenchymal transition at the ventral ectodermal ridge. *Development* 134(24):4315–4324. <https://doi.org/10.1242/dev.008151>
- Cano A, Perez-Moreno MA, Rodrigo I et al (2000) The transcription factor snail controls epithelial-mesenchymal transitions by repressing E-cadherin expression. *Nat Cell Biol* 2(2):76–83. <https://doi.org/10.1038/35000025>
- Kovacic JC, Mercader N, Torres M, Boehm M, Fuster V (2012) Epithelial- and endothelial- to mesenchymal transition: from cardiovascular development to disease. *Circulation* 125(14):1795–1808. <https://doi.org/10.1161/CIRCULATIONAHA.111.040352>
- Medici D, Potenta S, Kalluri R (2011) Transforming growth factor- $\beta$ 2 promotes Snail-mediated endothelial-mesenchymal transition through convergence of Smad-dependent and Smad independent signaling. *Biochem J* 437(3):515–520. <https://doi.org/10.1042/BJ20101500>
- Rinn JL, Chang HY (2012) Genome regulation by long noncoding RNAs. *Annu Rev Biochem* 81(1):145–166. <https://doi.org/10.1146/annurev-biochem-051410-092902>
- Fatica A, Bozzoni I (2014) Long non-coding RNAs: new players in cell differentiation and development. *Nat Rev Genet* 15(1):7–21. <https://doi.org/10.1038/nrg3606>
- Nagano T, Fraser P (2011) No-nonsense functions for long noncoding RNAs. *Cell* 145(2):178–181. <https://doi.org/10.1016/j.cell.2011.03.014>
- Huarte M (2015) The emerging role of lncRNAs in cancer (2015). *Nat Med* 21(11):1253–1261. <https://doi.org/10.1038/nm.3981>

20. Yuan JH, Yang F, Wang F et al (2014) A long noncoding RNA activated by TGF-beta promotes the invasion-metastasis cascade in hepatocellular carcinoma. *Cancer Cell* 25(5):666–681. <https://doi.org/10.1016/j.ccr.2014.03.010>
21. Gabory A, Jammes H, Dandolo L (2010) The H19 locus: role of an imprinted noncoding RNA in growth and development. *Bioessays* 32(6):473–480. <https://doi.org/10.1002/bies.200900170>
22. Raveh E, Matouk IJ, Gilon M, Hochberg A (2015) The H19 long non-coding RNA in cancer initiation, progression and metastasis—a proposed unifying theory. *Mol Cancer* 14:1–14
23. Zhang L, Yang F, Yuan J et al (2013) Epigenetic activation of the MiR-200 family contributes to H19-mediated metastasis suppression in hepatocellular carcinoma. *Carcinogenesis* 34(3):577–586. <https://doi.org/10.1093/carcin/bgs381>
24. Zhuo C, Jiang R, Lin X, Shao M (2017) LncRNA H19 inhibits autophagy by epigenetically silencing of DIRAS3 in diabetic cardiomyopathy. *Oncotarget* 8(1):1429–1437. <https://doi.org/10.18632/oncotarget.13637>
25. McArthur K, Feng B, Wu Y, Chen S, Chakrabarti S (2011) MicroRNA-200b regulates vascular endothelial growth factor-mediated alterations in diabetic retinopathy. *Diabetes* 60(4):1314–1323. <https://doi.org/10.2337/db10-1557>
26. Cao Y, Feng B, Chen S, Chu Y, Chakrabarti S (2014) Mechanisms of endothelial to mesenchymal transition in the retina in diabetes. *Invest Ophthalmol Vis Sci* 55(11):7321–7331. <https://doi.org/10.1167/iovs.14-15167>
27. Feng B, Cao Y, Chen S et al (2016) miR-200b mediates endothelial-to-mesenchymal transition in diabetic cardiomyopathy. *Diabetes* 65:1–12
28. Zhu GH, Li R, Zeng Y, Zhou T, Xiong F, Zhu M (2018) MicroRNA-142-3p inhibits high-glucose-induced endothelial-to-mesenchymal transition through targeting TGF-β1/Smad pathway in primary human aortic endothelial cells. *Int J Clin Exp Pathol* 11:1208–1217
29. Srivastava M, Frolova E, Rottinghaus B et al (2003) Imprint control element-mediated secondary methylation imprints at the Igf2/H19 locus. *J Biol Chem* 278(8):5977–5983. <https://doi.org/10.1074/jbc.M208437200>
30. Thomas AA, Feng B, Chakrabarti S (2017) ANRIL: a regulator of VEGF in diabetic retinopathy. *Invest Ophthalmol Vis Sci* 58(1):470–480. <https://doi.org/10.1167/iovs.16-20569>
31. Khan ZA, Cukiernik M, Gonder JR, Chakrabarti S (2004) Oncofetal fibronectin in diabetic retinopathy. *Investig Ophthalmol Vis Sci* 45(1):287–295. <https://doi.org/10.1167/iovs.03-0540>
32. Biswas S, Thomas AA, Chen S et al (2018) MALAT1: an epigenetic regulator of inflammation in diabetic retinopathy. *Sci Rep* 8:1–15
33. Chang PY, Yang CM, Yang CH, Chen MS, Wang JY (2009) Pars plana vitrectomy for diabetic fibrovascular proliferation with and without internal limiting membrane peeling. *Eye* 23(4):960–965. <https://doi.org/10.1038/eye.2008.334>
34. Angi M, Kalirai H, Coupland SE, Damato BE, Semeraro F, Romano MR (2012) Proteomic analyses of vitreous humor. *Mediat Inflamm* 2012:1–7. <https://doi.org/10.1155/2012/148039>
35. Gordon AD, Biswas SS, Feng B, Chakrabarti S (2018) MALAT1: a regulator of inflammatory cytokines in diabetic retinopathy. *Endocrinol Diabetes Metab* 1:1–11
36. Wu Y, Zuo Y, Chakrabarti R, Feng B, Chen S, Chakrabarti S (2010) ERK5 contributes to VEGF alteration in diabetic retinopathy. *J Ophthalmol* 2010:1–11
37. Wu L, Derynck R (2009) Essential role of TGF-β signaling in glucose-induced cell hypertrophy. *Dev Cell* 17(1):35–48. <https://doi.org/10.1016/j.devcel.2009.05.010>
38. Tang R, Li Q, Lv L et al (2010) Angiotensin II mediates the high-glucose-induced endothelial-to-mesenchymal transition in human aortic endothelial cells. *Cardiovasc Diabetol* 9:1–7
39. Feit-Leichman RA, Kinouchi R, Takeda M et al (2005) Vascular damage in a mouse model of diabetic retinopathy: relation to neuronal and glial changes. *Invest Ophthalmol Vis Sci* 46(11):4281–4287. <https://doi.org/10.1167/iovs.04-1361>
40. Xu Q, Deng F, Qin Y et al (2016) Long non-coding RNA regulation of epithelial–mesenchymal transition in cancer metastasis. *Cell Death Dis* 7:1–10
41. Xiang Y, Zhang Y, Tang Y, Li Q (2017) MALAT1 modulates TGF-β1-induced endothelial-to-mesenchymal transition through down-regulation of miR-145. *Cell Physiol Biochem* 42(1):357–372. <https://doi.org/10.1159/000477479>
42. Neumann P, Jae N, Knau A et al (2018) The lncRNA GATA6-AS epigenetically regulates endothelial gene expression via interaction with LOXL2. *Nat Commun* 9:1–12
43. Liang WC, Fu WM, Wong CW et al (2015) The lncRNA H19 promotes epithelial to mesenchymal transition by functioning as miRNA sponges in colorectal cancer. *Oncotarget* 6(26):22513–22525. <https://doi.org/10.18632/oncotarget.4154>
44. Bakker W, Eringa EC, Sipkema P, van Hinsbergh VWM (2009) Endothelial dysfunction and diabetes: roles of hyperglycemia, impaired insulin signaling and obesity. *Cell Tissue Res* 335(1):165–189. <https://doi.org/10.1007/s00441-008-0685-6>
45. Popov D (2020) Endothelial cell dysfunction in hyperglycemia: phenotypic change, intracellular signaling modification, ultrastructural alteration, and potential clinical outcomes. In *J Diabetes Mellitus* 2:189–195
46. Biswas S, Chakrabarti S (2017) Pathogenetic mechanisms in diabetic retinopathy: from molecules to cells to tissues. In: Kartha CC, Ramachandran S, Pillai RM (eds) *Mechanisms of Vascular Defects in Diabetes Mellitus*, *Advances in Biochemistry in Health and Disease*, 1st edn. Springer, Cham, pp 209–247
47. Zeisberg EM, Tamavski O, Zeisberg M et al (2007) Endothelial-to-mesenchymal transition contributes to cardiac fibrosis. *Nat Med* 13(8):952–961. <https://doi.org/10.1038/nm1613>
48. Abu El-Asrar AM (2016) Endothelial-to-mesenchymal transition contributes to the myofibroblast population in proliferative diabetic retinopathy. *Saudi J Ophthalmol* 30(1):1–2. <https://doi.org/10.1016/j.sjopt.2016.01.005>
49. Abu El-Asrar AM, Struyf S, Kangave D, Van Damme J (2006) Chemokines in proliferative diabetic retinopathy and proliferative vitreoretinopathy. *Eur Cytokine Netw* 17(3):155–165
50. Peng H, Li Y, Wang C et al (2016) ROCK1 induces endothelial-to-mesenchymal transition in glomeruli to aggravate albuminuria in diabetic nephropathy. *Sci Rep* 6:1–10
51. Eisenberg LM, Markwald RR (1995) Molecular regulation of atrioventricular valvuloseptal morphogenesis. *Circ Res* 77(1):1–6. <https://doi.org/10.1161/01.RES.77.1.1>
52. Yan XC, Cao J, Liang L et al (2016) miR-342-5p is a Notch downstream molecule and regulates multiple angiogenic pathways including Notch, vascular endothelial growth factor and transforming growth factor signaling. *J Am Heart Assoc* 5:1–15
53. Pardali E, Sanchez-Duffhues G, Gomez-Puerto MC, Dijke P (2017) TGF-induced endothelial-mesenchymal transition in fibrotic diseases. *Int J Mol Sci* 18:1–22
54. Biswas S, Thomas AA, Chakrabarti S (2018) LncRNAs: proverbial genomic junk or key epigenetic regulators during cardiac fibrosis in diabetes? *Front Cardiovasc Med* 2018:1–13
55. Xu X, Tan X, Hulshoff MS, Wilhelmi T, Zeisberg M, Zeisberg EM (2016) Hypoxia-induced endothelial-mesenchymal transition is associated with RASAL1 promoter hypermethylation in human coronary endothelial cells. *FEBS Lett* 590(8):1222–1233. <https://doi.org/10.1002/1873-3468.12158>
56. Xu X, Tan X, Tampe B et al (2015) Epigenetic balance of aberrant Rasal1 promoter methylation and hydroxymethylation regulates

- cardiac fibrosis. *Cardiovasc Res* 105(3):279–291. <https://doi.org/10.1093/cvr/cvv015>
57. Lewandowski SL, Janardhan HP, Trivedi CM (2015) Histone deacetylase 3 coordinates deacetylase-independent epigenetic silencing of transforming growth factor- $\beta$ 1 (TGF- $\beta$ 1) to orchestrate second heart field development. *J Biol Chem* 290(45):27067–27089. <https://doi.org/10.1074/jbc.M115.684753>
58. Kim J (2018) MicroRNAs as critical regulators of the endothelial to mesenchymal transition in vascular biology. *BMB Rep* 51(2):65–72. <https://doi.org/10.5483/BMBRep.2018.51.2.011>
59. Cruz-Solbes AS (2017) Epithelial to mesenchymal transition (EMT) and endothelial to mesenchymal transition (EndMT): role and implications in kidney fibrosis. *Kidney Dev Disease* 60:345–372